10

Optimization of perfluorocarbon nanoemulsions for molecular imaging by ^{19}F MRI

Christoph Grapentin[1], Friederike Mayenfels[1], Sabine Barnert[1], Regine Süss[1], Rolf Schubert[1*], Sebastian Temme[2], Christoph Jacoby[2], Jürgen Schrader[2], Ulrich Flögel[2*]

[1] Department of Pharmaceutical Technology and Biopharmacy, Albert Ludwigs University, Hermann-Herder-Strasse 9, 79104 Freiburg, Germany
[2] Department of Molecular Cardiology, Heinrich Heine University, Universitätsstraße 1, 40225, Düsseldorf, Germany

Outline:

Introduction

Tracking fate and function of specific cell types by molecular imaging methods is of great importance for basic research and holds the potential to be clinically applied for initial diagnosis as well as the monitoring of subsequent pharmacological treatment. Key applications include visualization of the destiny of transplanted stem cells for regenerative therapies [1-6] or dendritic cells for cancer immunotherapy [7,8]. Furthermore, imaging of immune cells has received increasing attention over the last decades, since it has become clear that inflammation plays a major role in many diseases. In this context, macrophages emerged as an attractive target, because these cells are key effectors of both the progression and resolution of inflammation [9-14]. However, direct monitoring of these cells by non-invasive imaging methods requires labelling of these cells with contrast agents or genetic modifications (expression of reporter genes like GFP or luciferase) independent of which modality is used. Recently, optical techniques, bioluminescence, PET (positron emission tomography), SPECT (single photon emission computer tomography) or MRI (magnetic resonance imaging) have successfully been applied to visualize labelled macrophages at inflammatory sites [15]. Nevertheless, optical techniques and bioluminescence are not suitable for high resolution cell tracking, since these techniques – although very sensitive and specific – can not resolve the localization of labelled cells within an heterogeneous inner organ. SPECT/CT and PET/CT display an excellent contrast but require the administration of radioactive agents and the exposition to high doses of X-ray radiation. On the other hand, MRI displays high spatial resolution and superior contrast between soft tissues without the need for radioactivity or X-rays.

Imaging of macrophage immigration by MRI has so far been predominantly performed by use of iron oxide-based nanoparticles (SPIO = superparamagnetic iron oxide; USPIO ultrasmall superparamagnetic iron oxide) [16,17]. After intravenous (i.v.) administration, these particles are taken up by monocytes and macrophages and lead to a signal depletion in ^{1}H MRI upon infiltration of the labelled cells into the inflamed area [18]. However, interpretation of iron-oxide nanoparticle induced ^{1}H signal erasure is sometimes difficult, since susceptibility artefacts especially in the boundary zone between different tissues can also result in signal deprivation and therefore lead to misinterpretation. In addition, the iron-oxide nanoparticle deposition yields to the loss of precise anatomical information and absolute quantification is hampered because there is no linear relationship between signal depletion and iron-oxide content.

As an alternative emulsified perfluorocarbons (PFCs) – containing the stable fluorine isotope ^{19}F – recently emerged as promising contrast agents for cell tracking by ^{1}H/^{19}F MRI combining the anatomical information (^{1}H MRI) and the localization of ^{19}F-labelled target cells Similar to other nanoparticles, PFC nanoemulsions (PFC-NE) are phagocytosed by monocytes and macrophages after i.v. injection. PFC-labelled cells subsequently migrate into the inflamed area resulting in a local deposition of ^{19}F nuclei [19,20] (Figure 10.1). Due to the lack of any natural ^{19}F background in the body, detected ^{19}F signals show a high degree of specificity [21], while its sensitivity is close to that of the ^{1}H nucleus. After merging anatomical ^{1}H and cell-tracking ^{19}F images the exact anatomical location of the ^{19}F hot spot can be precisely determined (Figure 10.1). In particular for inflammation imaging this technique has been validated so far in a variety of disease models by several groups (Figure 10.1, lower panel) [19,22-33].

Although ^{19}F MRI is a promising tool for cell tracking and inflammation imaging, sensitivity is a critical concern. ^{19}F MRI requires several hundreds to thousands of labelled cells per voxel for detection [19-21,34]. On the other hand, increasing the ^{19}F load per cell by improving the phagocytic uptake of PFC

particles by monocytes/macrophages (or other cells) *in vivo* would significantly improve the detection limit of the ^{19}F MRI technique. However, this is currently hampered by the massive uptake of "conventional" PFC emulsions by the reticuloendothelial system (RES). After i.v. application, PFC nanoemulsion particles are coated by serum proteins, which not only enhance their uptake by blood monocytes, but also cause their fast removal from the circulation by the RES. Thus, the large fraction of PFC particles absorbed by the RES strongly obstructs an efficient loading of monocytes in the blood and limits the sensitivity of the ^{19}F MRI approach. Since the major determinants of nanoparticle uptake by phagocytotic cells are size and surface properties, we aimed at modifying these characteristics to increase the efficiency and specificity of PFC uptake by distinct cell types.

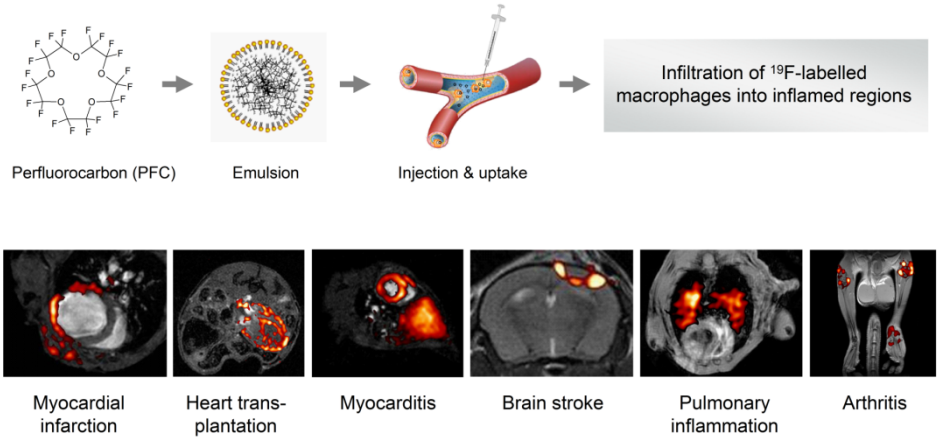

FIGURE 10.1
Principle of ^{19}F MRI inflammation imaging. Perfluorocarbons are emulsified to generate PFC-NE which can be injected intravenously. Emulsified particles are taken up by blood monocytes which immigrate into the inflamed area resulting in a localized ^{19}F signal. Merging of the anatomical ^{1}H grey scale image and the corresponding ^{19}F signal (red) reveals the exact anatomical position of infiltrated cells and thereby the inflamed area. This technique has been validated in a variety of clinically relevant disease models. Reprinted with permission from references [19,24-26,30]

Generation of stable PFC nanoemulsions with defined size

Perfluorocarbons are not mixible with water, therefore PFCs have to be dispersed in water or a physiological buffer system by the use of an emulsifying agent and energy input. As emulsifying compounds, lipids or poloxamers can be used to generate the PFC-NE by extrusion, ultrasound or high pressure homogenization. Nanoemulsions for parenteral application (e.g. labelling of immune cells) have to withstand heat sterilization or have to be produced under aseptic conditions. The droplet size of PFC-NE are preferentially of small dimensions (<200 nm), but depending of the nature of PFC, emulsifier and preparation technique, they are characterized by varying size distribution. To analyze the properties of PFC-NE photon correlation spectroscopy (PCS) or electron microscopy are routinely used. PCS yields the average hydrodynamic diameter and the polydispersity index (PI or PDI) that describes the size distribution. However, this method is limited to dispersions with a rather narrow size distribution [35].

Perfluorocarbons suited for ^{19}F MRI

PFCs are synthetic organic molecules where all hydrogen atoms have been replaced by fluorine atoms. The C-F- and C-C-bonds are exceptionally strong and the electronegativity of fluorine results in weak intermolecular forces as well as hydrophobic and lipophobic properties [36]. No enzyme is known to split PFCs and no biological PFC degradation pathway has been reported up to now. PFCs are therefore regarded as non-toxic, biochemically inert compounds. PFCs usually display a large density of about 2 g/ml [37]. They show a high dissolution capacity for gases and were intensely investigated as oxygen carriers in the 1960s [38]. In the following decades a multitude of nanoemulsions have been developed for the use as blood substitutes but also as medical contrast agents, but none has been established on the market. Among the problems encountered with PFC-NE were insufficient size stability upon storage, activation of the complement system or other safety and stability concerns [39].

For MRI purposes, the most widely used PFCs are perfluoro-15-crown-5 ether (PFCE), perfluorooctyl bromide (PFOB) and perfluorodecaline (PFD), whose chemical structures are shown in Figure 10.2. Due to its 20 chemically and magnetically equivalent fluorine nuclei, PFCE is characterized by a single MR resonance and therefore has ideal properties for MR imaging techniques, but it exhibits an extremely long biological half-life and is therefore not suitable for clinical applications [37]. PFD and PFOB have short biological half-lives but cannot be imaged by conventional methods without artefacts [40]. Of note, PFOB has a terminal bromine that alters its chemical behavior to slightly lipophilic, thus simplifying the manufacture of stable nanoemulsions and facilitating its passage over membrane barriers which contributes to its quick release from the body. Perfluorohexyloctane (F6H8) represents the class of mixed hydrocarbon-fluorocarbons, or semifluorinated alkanes. Although, it has not yet been used for MR imaging, it is an interesting candidate, since it is already clinically approved as long-term tamponade in complicated retinal detachments and as an intraoperative instrument for retinal surgery. Another important property is it its significantly lower density (1.35 g/ml) compared to the perfluorocarbons.

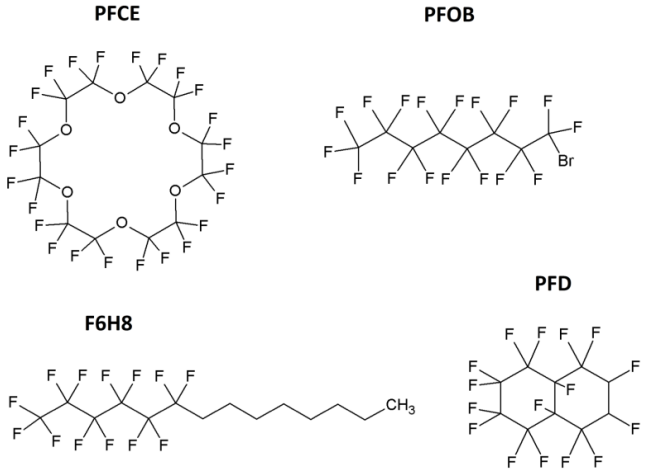

FIGURE 10.2
Perfluorocarbons for the generation of PFC-NE. Chemical structures of different PFCs which can be used for the generation of PFC-NE. PFCE has 20 chemically and magnetically equivalent fluorine atoms which makes it ideally suitable for conventional ^{19}F MRI but has a very long tissue retention time. PFD and PFOB are characterized by a short biological half-life but exhibit complex spectra requiring dedicated imaging sequences [40]. F6H8 is a semifluorinated alkane which has not yet been used for MR imaging

Emulsifiers and nanoemulsions

For later pharmaceutical approval, the emulsifiers should already be certificated for i.v. application. With regard to this, both phospholipids and poloxamers are validated substances. Phospholipids are naturally occuring reagents and show a good biocompatibility. They can be produced cost efficiently from well known sources, like egg yolk or soy bean. Phospholipids easily form nanoemulsions with PFCs, but are prone to hydrolysis and oxidation – factors that limit the stability of NE particles. However, the main disadvantage of phospholipids is the additional formation of "empty" liposomes. Liposomes do not contain any PFCs and impair the stability of the nanoemulsion. Poloxamers are block polymers of an A-B-A type, poly(ethylenglycol)-poly(propylenglycol)-poly(ethylenglycol). Poloxamers can be produced in large scale, but due to their relative low surface activity they must be used in higher amounts and tend to form highly viscous dispersions. Another important disadvantage is a possible activation of the complement system [41]. In our hands, phosholipids are superior to poloxamers for the generation of PFC-NE.

Manufacturing perfluorocarbon nanoemulsions (PFC-NE)

Because of the quite different physical and chemical properties of the starting ingredients, high energy inputs are required for the formation of PFC-NE and to reach a fine dispersion of the PFC in aqueous solutions. This can be achieved by high pressure homogenization, sonication or extrusion. In all cases, as a first step a crude emulsion (µm size) is produced by means of high shear mixing. Sonication is limited to small scale production whereas bigger scales of several 100 ml can be produced with extrusion. Both methods usually lead to a high content of liposomes and NE droplets of a wide size distribution. The most suitable way to manufacture PFC-NE with a low liposome content and acceptable size distribution is high pressure homogenization which can be scaled up to large industrial magnitudes.

High pressure homogenization for the generation of PFC-NE with different size

To generate PFC emulsion particles with different average size, we altered the ratio of the PFC (F6H8, PFD and PFOB were tested) and phospholipid (here S75; S = soy) – the higher the PFC amount, the larger the particles. This is because less emulsifier is available to stabilize the inner PFC phase. The preformed rough emulsions are then subjected to high pressure homogenization (e.g. Avestin, Emulsiflex C5). By passing a narrow valve, pressures up to 1500 bar are created that disrupt the µm size droplets of the crude emulsion. Droplet size decreases each time the emulsion passes the valve. By modifying the ratio of PFC and S75 in the range of 1 to 50, particles with a mean diameter of 100 to 300 nm can be generated (Figure 10.3). However, these preparations show a varying size distribution with a polydispersity index (PDI) between 0.46 and 0.1 (data not shown). Although differences between individual PFCs were observed, this technique seems to be suitable for all PFCs investigated and also be applicable for other PFCs.

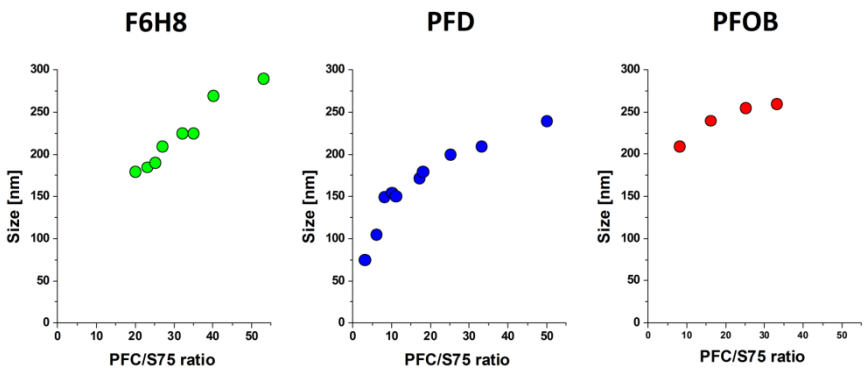

FIGURE 10.3
Dependence of PFC-NE size from PFC/emulsifier ratio. PFC emulsions were prepared by altering the ratio of emulsifier and perfluorocarbon (PFD, F6H8, PFOB) and subsequent high pressure homogenization (700 bar, 10 cycles)

Removal of liposomes from perflurocarbon nanoemulsions

Liposomes do not contain PFCs but compete with PFC-NE droplets for cellular uptake leading to a decreased ^{19}F loading of target cells and thereby to a loss of sensitivity for *in vivo* cell tracking. Since PFC-NE have a high density, we separated NE droplets from liposomes by repeated centrifugation, e.g. 25 min at 13,000 g for three times. Figure 10.4 shows electron microscopic images of a PFC-NE before centrifugation (left) as well as the resuspended pellet (right) and the supernatant (middle) after centrifugation. On the left, empty liposomes can clearly be recognized, which were almost completely removed upon repeated centrifugation (right). The pictures also show that PFC nanoemulsions are usually characterized by particles of varying size. The mean diameter and the obtained size distribution depend on the emulsifier, the homogenization process (pressure and cycles) as well as on the PFC used and its percentage (see above).

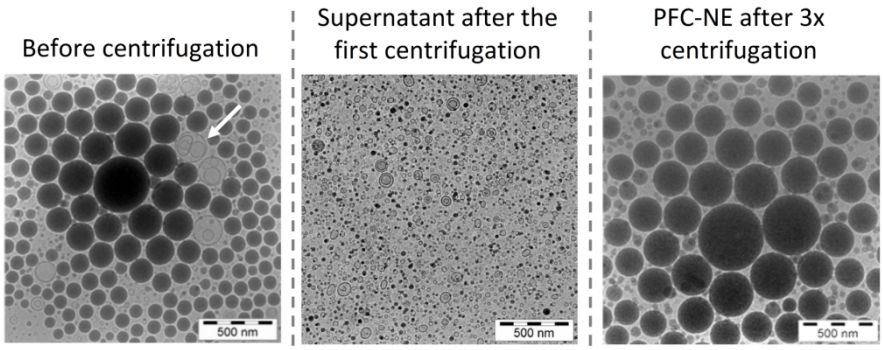

FIGURE 10.4
Removal of liposomes by repeated centrifugation. Electron microscopy of PFC emulsion before and after centrifugation (3 times 13,000 g) as well as of supernatant after the first centrifugation step. The arrow indicates liposomes without PFC content. NE droplets appear dark because of their PFC load, while empty liposomes are bright

Stability of PFC nanoemulsions

Stability is a critical issue for the manufacturing of PFC-NE. At higher temperatures, coalescence, i.e. the irreversible fusion of two or more droplets to a bigger one, is the main mechanism of instability. Over a longer storage period molecular diffusion, also called Ostwald Ripening, triggers the irreversible growth of a droplet, at the expense of the smaller ones. Molecular diffusion can be diminished by the addition of a PFC homologue of lower water solubility, e.g. admixing of small amounts of perfluorodecyl bromide to perfluorooctyl bromide before homogenization [42]. Another method to obtain more stable nanoemulsions is to incorporate semifluorinated alkanes as co-surfactants which generate a stabilizing bridge beween lipids and PFCs [41]. Furthermore, type of PFC and emulsifier as well as the ratio of both components are factors that critically affect emulsion stability. Of note, the properties of the aqueous phase also impact on stability, since phospholipids hydrolyze more easily at elevated pH values and oxidation occurs already at trace amounts of metals. The latter could be avoided by incorporation of metal chelators like EDTA and antioxidants (i.e. tocopherol), but this would hamper the biocompatibility of the emulsion. However, PFC-NE should always be prepared with a degased buffer to prevent oxygen in the formulation. Nevertheless, when stored at 4 °C we observed properly prepared PFC-NE to be quite stable even without any additives. Figure 10.5 shows excellent stability for all tested nanoemulsions except for those with a low amount of phospholipid (e.g. PFOB emulsified with 15.8 mM S75).

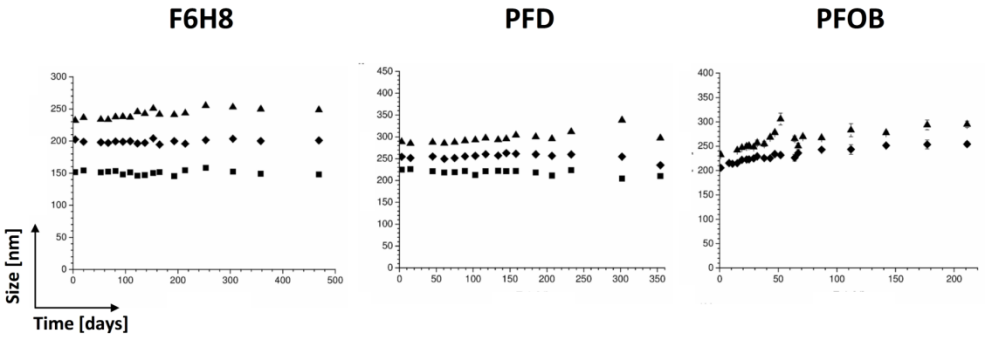

FIGURE 10.5 Long-term stability of different PFC-NE. Stability of F6H8-NE (40% PFC), PFD-NE (20% PFC) and PFOB-NE (20% PFC). ▲= 15.8 mM S75, ■= 31.6 mM S75, ♦ = 47.4 mM S75

Size exclusion chromatography (SEC)

The uptake of nanoparticles by phagocytic cells is critically dependent on their respective size. Thus, development of a nanoemulsion should focus on droplets with a well defined size, i.e. with a narrow size distribution. Otherwise, contaminations with droplets of large size that are taken up more efficiently and/or carry a higher PFC load may affect both the specificity and quantity of the PFC label. As can be derived from Figure 10.4, PFC-NE generated by use of phospholipids usually show a broad size distribution – a problem which cannot be overcome by the conventional manufacturing process. However, the formation of defined PFC-NE is feasible by combining centrifugation (see above) with size exclusion chromatography (SEC). Figure 10.6 shows that we were able to successfully separate well defined fractions of a PFD emulsion *via* a Toyopearl HW-75S column. Fraction collection in custom intervals (Figure 10.6A) enabled the isolation of distinct PFC-NE with different sizes and a very narrow size distribution (PDI of 0.07 after SEC; Figure 10.6B).

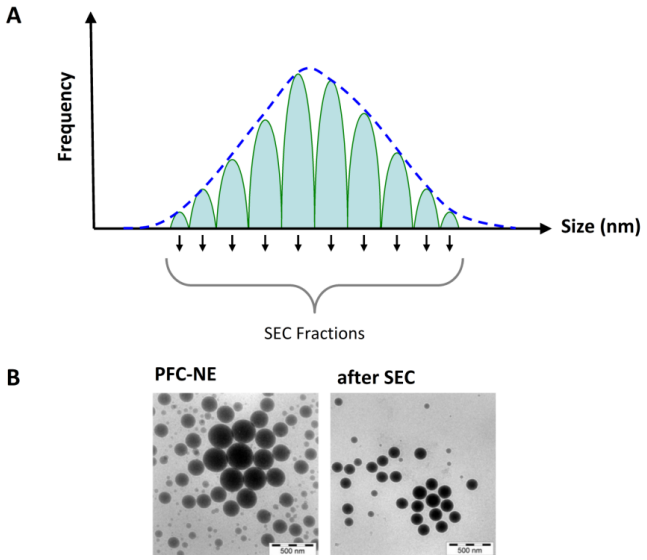

FIGURE 10.6
Isolation of SEC fractions with defined size and very low PDI. A) Fraction collection leads to PFC-NE of defined size. B) Electron microscopy of PFC emulsion before and after size exclusion chromatography (SEC). PFCs are displayed with average size of 187 nm and a polydispersity index (PDI) of 0.14 (before SEC) and a size of 180 nm and a PDI of 0.07 (after SEC)

Uptake of PFC Nanoemulsions by Macrophages

Surface characteristics [43], geometry [44] and size [45] are the most important factors which determine nanoparticle uptake by phagocytes (and other cells). In general, larger particles are taken up more efficiently by phagocytes than smaller ones, which has been primarily demonstrated by *in vitro* uptake investigations with latex beads of distinct sizes. However, almost no systematic studies have been carried out on the dependence of cellular PFC-NE incorporation from particle size, most likely due to the difficulties that occur in producing these NE with a narrow size distribution.

Size and concentration dependent uptake

To investigate the cellular uptake of PFC-NE with different size the murine peritoneal macrophage cell line J774.A1 was used, which is an established model for primary macrophages [45]. For analysis of uptake, cells were incubated under defined conditions (100,000 cells, 500 µl medium, 2 h, 37 °C) with rhodamine-labelled PFD nanoemulsions of distinct particle size (generated with SEC; see previous section) and nanodroplet incorporation was quantifed by flow cytometry *via* their rhodamine signal. As shown in Figure 10.7A, the uptake of PFC nanoparticles by this cell type rises with increasing size. Interestingly, a sigmoid curve was observed for the size-dependent particle uptake by J774.A1 macrophages. Particles smaller than 200 nm were phagocytosed only to a minor amount. However, the uptake steeply increases for particles larger than 200 nm in diameter and reaches a plateau for PFC

particles bigger than 300 nm. These findings confirm that uptake of PFC-NE by macrophages can be governed by the particle size, which thus can be used as a passive targeting strategy.

In a further step, we investigated whether besides size also the concentration of the nanoemulsion impacts on PFC uptake by J774.A1 macrophages. Again, cells were incubated under strictly defined conditions (see above) with rhodamine-labelled NE fractions of three different sizes and stepwise increasing concentrations. Subsequent quantification of the fluorescence signal by flow cytometry showed that for all individual preparations droplet incorporation followed an exponential increase with varying slope depending on particle size. As can be seen in Figure 10.7B, 180-nm nanodroplets exhibit a maximum uptake of about 60% positive cells. The EC_{50} (half-maximal effective concentration) value for this size was determined to be 170 nmol. Particles with a diameter of 239 nm led to about 80% positive cells and an EC_{50} value of 80 nmol, whereas particles with a size of 345 nm showed a further increased uptake to ~ 90% PFC-loaded cells and an EC_{50} value of 10-20 nmol (Figure 10.7B).

Taken together these experiments demonstrate that the incorporation of PFC-NE by macrophages can be manipulated by both size and concentration.

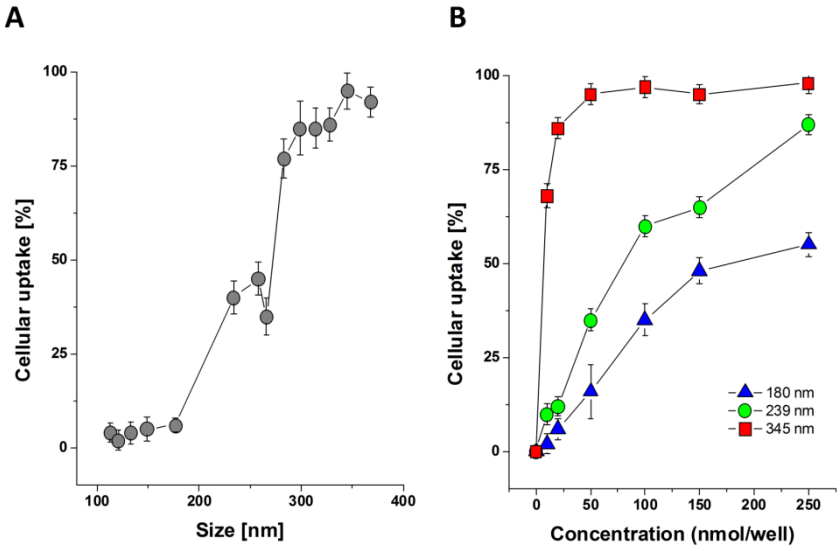

FIGURE 10.7
Dependence of PFC nanoparticle uptake from size and concentration: A) Uptake of PFC emulsion particles of different size by J774.A1 macrophages, 150 nmol droplets per 100,000 cells. B) Concentration-dependent uptake of PFC emulsion by J774.A1 cells. All data are given as mean values ± SD from n=3-4 independent experiments

Site-specific delivery of Perfluorocarbon Nanoemulsions

The "passive" uptake of PFC-NE (generated as described above) by cells of the innate immune system can be easily exploited to identify inflamed tissues by ^{19}F MRI detection of infiltrated, PFC-loaded immune cells (see introduction). A more specific targeting of PFC-NE is required to visualize cells which under normal conditions are labelled only to a low extent (e.g. B-cells) or which are not labelled at all

by PFC-NE (like T-cells or platelets). To this end, the surface of the NE has to be equipped with a site-specific antigen that directs it to its target [46]. At the same time the normal "passive" phagocytosis of those particles must be prevented to enhance sensitivity and ensure specificity of the detected ^{19}F signal.

PEGylation of PFC-NE to reduce phagocytic uptake

After intravenous injection, nanoparticles are coated by serum proteins (so-called opsonisation) which facilitates the uptake by immune cells. A well-known procedure to impair the attachment of serum proteins to nanoparticles is the coupling of polyethyleneglycol (PEG) to their surface. PEGylation has been applied to a variety of nanoparticles to reduce opsonization and to delay their clearance from the bloodstream [47]. Interestingly, PEGylated nanoparticles have already been used for tumor imaging, in that the extended persistence in the circulation prolongs the temporal window for passive diffusion through leaky endothelium which leads to an increased deposition of nanoparticles at the tumor site [48,49].

For liposomes or nanoemulsions, usually a PEG-modified phospholipid (e.g. distearoylglycero-phosphoethanolamine-methoxy-PEG) is incorporated during the homogenization process. However, we used a post-insertion attempt in which the nanoemulsion is modified with a sterol-PEG after its preparation. Sterol-PEGs can easily be inserted into the preformed phospholipid layer of the nanoemulsion and have been previously used to modify liposomes [50]. To verify whether sterol-PEGylation also leads to a stealth effect for our PFC-NE, a PFD-NE with a size of 229 nm (PDI 0.21) was prepared and modified with different amounts of a sterol-PEG_{1300}. Afterwards, the cellular uptake of rhodamine-labelled PFC-NE and PFC-PEG-NE particles was compared by flow cytometry. Figure 10.8A demonstrates that after 2 h of incubation at 37 °C unmodified nanoparticles ("blank") were internalized by 85% of the cells, while PEGylation decreased this value to 10% (for 5 mol% PEG) and 2% (for 10 mol% PEG), respectively. Importantly, PEGylation also strongly reduced cellular uptake of PFC nanoemulsions with larger droplet size: When 5 mol% sterol-PEG_{1300} was inserted into PFC particles with a mean diameter of 320 nm and a PDI of 0.13, the cellular uptake of this preparation was diminished to about 2% (data not shown).

In a next step, we analyzed whether PEGylation of PFC nanoparticles also impacts on the phagocytosis by the reticuloendothelial system *in vivo*. For this, the biodistribution of the ^{19}F signal in murine blood, spleen, and liver was monitored by ^{19}F MRI starting 30 min after PFC application up to 4 h after injection. A chemical shift imaging (CSI) technique was applied for artefact-free detection of the used PFOB-NE [40]. Figure 10.8B shows representative images acquired in two separate experiments when animals where exposed to PEGylated (bottom) and non-PEGylated (top) emulsions, respectively.

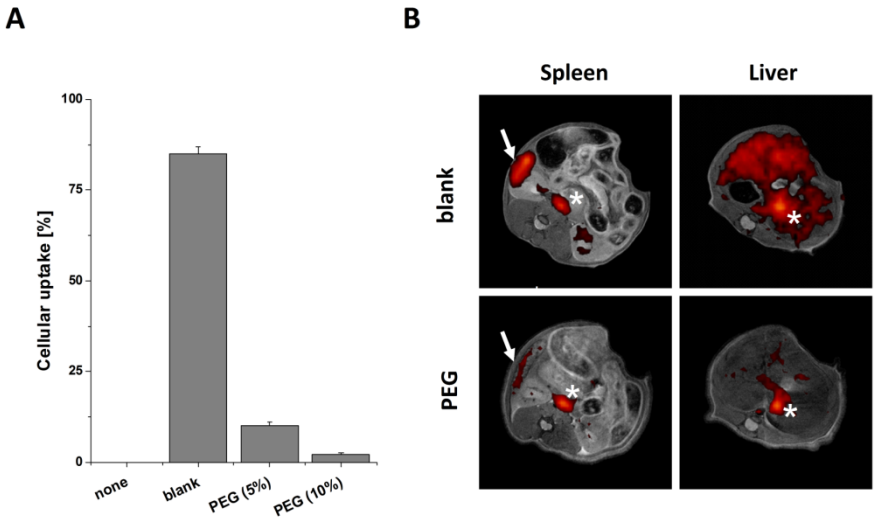

FIGURE 10.8
Impact of PEGylation on PFC uptake in vitro and in vivo
A) PEGylation reduces cellular uptake by J774.A1 cells. J774.A1 cells were incubated with rhodamine-labelled PEGylated and non-PEGylated PFC emulsion particles for 2 h and analyzed by flow cytometry. **B)** Representative images displaying the ^{19}F signal of PEGylated (bottom) and non-PEGylated (top) droplets in liver (right) and spleen (left) 30 min after injection. Arrows point to location of the spleen; asterisks indicate the position of blood vessels (i.e. abdominal aorta and vena cava inverior). 100 µl of PFOB emulsion were injected into the tail vein and subsequently analyzed by ^{1}H/^{19}F MRI

Although the ^{19}F signal in the blood (asterisks) was similar for both preparations 30 min after injection, the fluorine signal of PEGylated nanoemulsions was hardly detectable in liver and strongly reduced in the spleen (arrows) as compared to non-PEGylated emulsions. Quantification of the data revealed a significant retarded uptake of PEGylated droplets by liver and spleen compared to non-PEGylated nanoemulsions at this time (n=3, P<0.05). Two hours post injection, the signal in the liver was still 3.5-fold higher for non-PEGylated nanoemulsions. Interestingly, the ^{19}F signal-to-noise ratio (SNR) in the blood showed the largest difference between PEGylated and non-PEGylated PFCs after 2 h, with a 1.5-fold higher SNR for PEGylated PFCs. However, 4 h after injection the ^{19}F signal in the blood was similar for the two PFC emulsions and deposition of PEGylated PFCs was slightly elevated in spleen but much higher in liver compared to non-PEGylated nanoemulsions. After 24 h both emulsions were fully cleared from blood, and the ^{19}F signal in liver and spleen was identical between PEGylated and non-PEGylated emulsions (data not shown).

Altogether, the data show that sterol-PEGylation of PFC-NE almost abolishes the cellular uptake by J774.A1 macrophages *in vitro* and delays the deposition of ^{19}F in liver and spleen *in vivo*. However, several hours after injection the ^{19}F content in liver and spleen were slightly elevated compared to non-PEGylated nanoemulsion droplets, which can be explained by the longer circulation of the PEGylated nanoparticles [51]. The fact that PEGylation delays but does not totally inhibit the PFC uptake by liver and spleen can be related to the decreased kinetics of serum protein adsorption to the PEGylated PFC nanoparticles which usually would facilitate their removal from the bloodstream and diminish the contact time between particles and these organs.

Antibody-mediated active targeting of PFC-NE

For site-specific targeting of nanocarriers, ligands are coupled to the particle surface, which are mostly either of peptidic nature or small organic molecules, although other structures are possible as well. For PFC-NE a targeting via antibodies [52], RGD peptide [53] or folate [54] has been reported. In the following, we extend the sterol-PEGylation of preformed PFC-NE (described above) to generate cell-type-specific contrast agents. In a first step, as a proof-of-concept we "rescued" the particle uptake capability of macrophages for PEGylated PFC-NE by coupling of an antibody directed against the scavenger receptor A. In another model, we modified PFC-NE with a single chain antibody for the activated gpIIb/IIIa receptor to direct them specifically to activated platelets which under normal conditions do not exhibit any affinity towards PFC nanoparticles.

For coupling of ligands to the PFC-NE, we synthesized sterol-PEGs with a reactive N-hydroxysuccinimide group (NHS) at the distal end of the PEG-chain, yielding a sterol-PEG-NHS-reagent. Anti-CD204 antibody (raised against scavenger receptor A) can easily be attached to this construct *via* covalent linking of amine groups to the NHS-group. The sterol-PEG-antibody is subsequently inserted into the phospholipid monolayer of the PFC-NE. As untargeted control, neat sterol-PEG-NEs were used. Figure 10.9 summarizes the data which were obtained after incubation of J774.A1 macrophages with the different rhodamine-labelled PFC-NEs. While the unmodified PEGylated nanemulsion ("PEG") was again taken up only by a minority of the cells, the anti-CD204 targeted emulsion ("CD204Ab") was internalized by approximately 80% of the J774.A1 macrophages.

In the next step, we aimed at targeting activated platelets as key players in plaque rupture. Early and non-invasive detection of platelets on micro-atherothromboses would provide a means to identify unstable plaques and thereby allowing prophylactic treatment towards prevention of stroke or myocardial infarction. However, platelets are not known to exhibit any phagocytic properties which might be exploited for internalization of contrast agents enabling their tracking by molecular imaging methods *in vivo*.

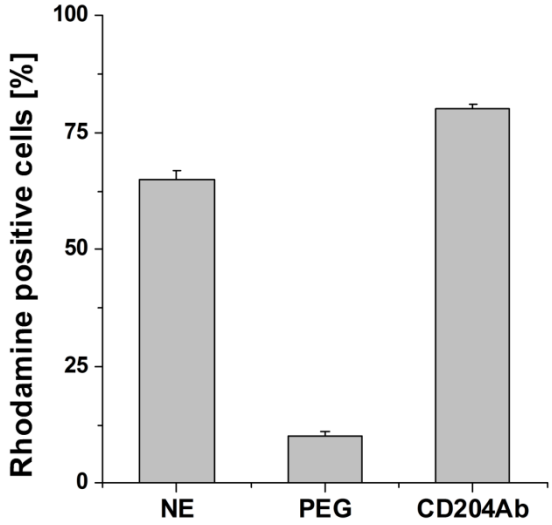

FIGURE 10. 9
Specific uptake of PFC-NE by coupling of an anti-CD204 antibody. Bars represent mean values ± SD from n=3 independent experiments

A promising option for selective direction of PFC-NE to this non-phagocytic target population seemed to be the coupling of antibodies raised against the activated gpIIb/IIIa receptor which is predominantly expressed on activated platelets. For this purpose, complete IgGs are not the first choice for *in vivo* applications, mainly because of their presence of the Fc-part which might result in recognition by Fc-receptors on macrophages, B-cells, NK-cells or activation of the complement system as well as induction of adaptive immune responses. Therefore, we modified PFC-NE with the well-characterized single chain antibody LB24, which has already been successfully applied *in vivo* for detection of thrombii in mouse carotid-arteries using ultrasound [55]. Subsequently, we analyzed the cellular association of the modified, rhodamine-labelled PFC-NE to clon3 cells, which constitutively express the activated form of the gpIIb/IIIa receptor. As control, we used the non-specific single chain antibody LB46 and A5 cells, respectively, which do not express the activated form of the receptor. Figure 10.10 shows that this targeting strategy resulted specifically in clon3 cells in an almost 10-fold increased uptake of LB24-coupled PFC-NE as compared to LB46-PFC-NE controls.

In summary, these results demonstrate that sterol-PEGs with chemically reactive end groups can serve as versatile tools to (i) stealth preformed PFC-NE for rapid uptake by the reticuloendothelial system and (ii) equip them with site-specific ligands against cells or structures which normally could not be labelled. The described post-insertion technique offers the unique advantage that also antibodies or other thermodynamically less stable compounds could be coupled to the PFC-NE, which might be otherwise destroyed or at least modified by either high pressure homogenization or the subsequent autoclavation process for sterilization of the nanoparticles.

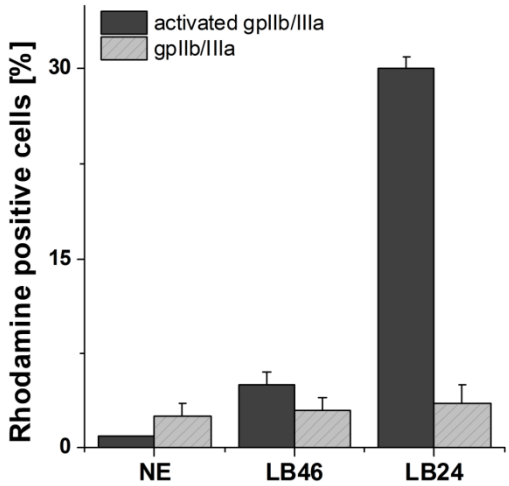

FIGURE 10.10
Specific targeting of PFC-NE against activated platelets. LB24 targeting to the activated gpIIb/IIIa receptor in clon3 cells (black bars). As control, the non-specific antibody LB46 and A5 cells (striped bars), which do not express the activated form of the receptor were used. Data represent mean values ± SD from n=3 independent experiments

Perspectives and Conclusions

Since perfluorocarbons are non-toxic and can be emulsified with pharmaceutically approved phospholipids, obtained PFC-NE are promising contrast agents for (immune) cell tracking by ^{19}F MRI in the clinical setting. ^{19}F MRI in combination with intravenously administered emulsified PFCs has already been successfully applied for imaging of macrophage infiltration during myocardial and cerebral ischemia [19], lipopolysaccharide-induced lung injury [24], bacterial abscess formation [27] and collagen-induced arthritis [26]. This approach was also applied to monitor anti-inflammatory treatment during transplant rejection and collagen-induced arthritis [25,26]. A further step towards a clinical application has recently been made when it could be shown that PFCs with short biological half lives are suitable for inflammation imaging [40]. Although this approach is highly specific due to the lack of any ^{19}F background in the body, sensitivity is a key concern. Several hundreds to thousand PFC-loaded cells are required in the area of interest for detection by ^{19}F MRI [19,34]. Sensitivity is even more relevant for PFCs with short biological half live, since they display complex ^{19}F spectra resulting in a loss of signal-to-noise during data acquisition and analysis compared to the ideal PFC for ^{19}F MRI, i.e. perfluoro-15-crown-5 ether [34,40]. Therefore, an efficient direction of PFC particles to the target cell type is highly desirable, which is currently hampered by the massive uptake of conventional PFC emulsions by the reticuloendothelial system.

Passive targeting to macrophages can be achieved by applying NE of distinct sizes. Formation of PFC-NE with different sizes revealed that particles <200 nm in diameter were less efficiently taken up by macrophages, while droplets with a diameter of >300 nm resulted in a massive increase in PFC uptake. Thus, we developed a protocol for the generation of distinct PFC emulsion particles with very narrow size distribution by modifying the ratio of perfluorocarbon/emusifier and subsequent fractionation by size exclusion chromatography. The dependency of the particle size from the PFC/emulsifier ratio is due to the alteration in total surface area to volume. However, there are limits for the smallest and largest particle sizes. The maximum size is determined by the amount of emulsifier which is sufficient to stabilize the dispersed phase. Further increases of the ratios will result in leakage of membrane curvature and instable particle preparations. Lowering the minimum size results in increased membrane curvature, which results in membrane stress. Therefore, further addition of the emulsifier will not decrease particle size but lead to the formation of micelles or liposomes.

PEGylation of PFC emulsion particles nearly abolished the cellular uptake, which could be reconstituted by coupling of a specific antibody recognizing a specific scavenger receptor on macrophages. Thus, both site specific targeting and prevention of uptake by the reticuloendothelial system can be reached by modifying the nanoemulsions with a PEG-shield and equipping this with specific ligands. Of note, the described post-insertion technique can also be applied to antibodies or other thermodynamically unstable compounds, since the coupling is carried out after high pressure homogenization and autoclavation of PFC-NE.

Although the present study has mainly focused on detecting specifically macrophages by ^{19}F MRI, the strategy of optimizing PFC targeting may as well be useful for other cell populations as shown for the direction of PFC-NE to activated platelets. ^{19}F MRI has been applied to detect stem cell homing [34], T-cell infiltration [56,57] and migration of dendritic cells [58] after *ex vivo* labelling of these cells. Therefore, the presented approach might enable a specific tracking of these cells *in vivo*, too. In addition, our targeting technique could also improve *ex vivo* labelling of cells for subsequent transplantation, since distinct cells within a mixture of populations could be selected. Finally, the extended temporal window provided by the addition of PEG to the particles surface can be exploited to

specifically direct PFCs to cells or structures apart from both the reticuloendothelial system and monocytes/macrophages *in vivo,* which could strongly expand possible applications for ^{19}F MRI.

Acknowledgments

The authors thank Bodo Steckel and Nicole Specht for excellent technical assistance and Prof. Karlheinz Peter (Melbourne, Australia) for kindly providing us with the LB24 and LB46 single chain antibodies. This study was supported by the Deutsche Forschungsgemeinschaft (DFG), subproject Z2 of the Sonderforschungsbereich 612 and grant SCHR 154/13-1.

References

1. Adamczak J., Hoehn M. In vivo imaging of cell transplants in experimental ischemia. Prog. Brain Res. 2012; 201 55-78.
2. Lu S. S., Liu S., Zu Q. Q., Xu X. Q., Yu J., Wang J. W., Zhang Y., Shi H. B. In vivo MR imaging of intraarterially delivered magnetically labeled mesenchymal stem cells in a canine stroke model. PLoS One 2013; 8(2) e54963.
3. Mangoni M., Livi L., Biti G., Di C., V, Capaccioli N., Castier Y., Loriot Y., Mordant P., Deutsch E. Stem cell tracking: toward clinical application in oncology? Tumori. 2012; 98(5) 535-542.
4. Qi Y., Feng G., Huang Z., Yan W. The application of super paramagnetic iron oxide-labeled mesenchymal stem cells in cell-based therapy. Mol. Biol. Rep. 2012; 40(3) 2733-2740.
5. Shen Y., Shao Y., He H., Tan Y., Tian X., Xie F., Li L. Gadolinium(3+)-doped mesoporous silica nanoparticles as a potential magnetic resonance tracer for monitoring the migration of stem cells in vivo. Int. J. Nanomedicine. 2013; 8) 119-127.
6. Srinivas M., Boehm-Sturm P., Figdor C. G., de Vries I. J., Hoehn M. Labeling cells for in vivo tracking using (19)F MRI. Biomaterials. 2012; 33(34) 8830-8840.
7. de Vries I. J., Lesterhuis W. J., Barentsz J. O., Verdijk P., van Krieken J. H., Boerman O. C., Oyen W. J., Bonenkamp J. J., Boezeman J. B., Adema G. J., Bulte J. W., Scheenen T. W., Punt C. J., Heerschap A., Figdor C. G. Magnetic resonance tracking of dendritic cells in melanoma patients for monitoring of cellular therapy. Nat. Biotechnol. 2005; 23(11) 1407-1413.
8. Srinivas M., Aarntzen E. H., Bulte J. W., Oyen W. J., Heerschap A., de Vries I. J., Figdor C. G. Imaging of cellular therapies. Adv. Drug Deliv. Rev. 2010; 62(11) 1080-1093.
9. DiPietro L. A. Wound healing: the role of the macrophage and other immune cells. Shock 1995; 4(4) 233-240.
10. Lucas T., Waisman A., Ranjan R., Roes J., Krieg T., Muller W., Roers A., Eming S. A. Differential roles of macrophages in diverse phases of skin repair. J. Immunol. 2010; 184(7) 3964-3977.
11. Mosser D. M., Edwards J. P. Exploring the full spectrum of macrophage activation. Nat. Rev. Immunol. 2008; 8(12) 958-969.

12. Shi C., Pamer E. G. Monocyte recruitment during infection and inflammation. Nat. Rev. Immunol. 2011; 11(11) 762-774.

13. Soehnlein O., Lindbom L. Phagocyte partnership during the onset and resolution of inflammation. Nat. Rev. Immunol. 2010; 10(6) 427-439.

14. Yona S., Jung S. Monocytes: subsets, origins, fates and functions. Curr. Opin. Hematol. 2010; 17(1) 53-59.

15. Dorward D. A., Lucas C. D., Rossi A. G., Haslett C., Dhaliwal K. Imaging inflammation: Molecular strategies to visualize key components of the inflammatory cascade, from initiation to resolution. Pharmacology & Therapeutics 2012; 135(2) 182-199.

16. Stoll G., Bendszus M. Imaging of inflammation in the peripheral and central nervous system by magnetic resonance imaging. Neuroscience 2009; 158(3) 1151-1160.

17. Yilmaz A., Rosch S., Klingel K., Kandolf R., Helluy X., Hiller K. H., Jakob P. M., Sechtem U. Magnetic resonance imaging (MRI) of inflamed myocardium using iron oxide nanoparticles in patients with acute myocardial infarction - Preliminary results. Int. J. Cardiol. 2013; 163(2) 175-182.

18. Stoll G., Bendszus M. New approaches to neuroimaging of central nervous system inflammation. Curr. Opin. Neurol. 2010; 23(3) 282-286.

19. Flögel U., Ding Z., Hardung H., Jander S., Reichmann G., Jacoby C., Schubert R., Schrader J. In vivo monitoring of inflammation after cardiac and cerebral ischemia by fluorine magnetic resonance imaging. Circulation 2008; 118(2) 140-148.

20. Temme S., Bönner F., Schrader J., Flögel U. ^{19}F magnetic resonance imaging of endogenous macrophages in inflammation. Wiley Interdiscip. Rev. Nanomed. Nanobiotechnol. 2012; 4(3) 329-343.

21. Ruiz-Cabello J., Barnett B. P., Bottomley P. A., Bulte J. W. Fluorine (^{19}F) MRS and MRI in biomedicine. NMR Biomed. 2011; 24(2) 114-129.

22. Balducci A., Helfer B. M., Ahrens E. T., O'Hanlon C. F. III, Wesa A. K. Visualizing arthritic inflammation and therapeutic response by fluorine-19 magnetic resonance imaging (19F MRI). J. Inflamm. (Lond) 2012; 9(1) 24.

23. Balducci A., Wen Y., Zhang Y., Helfer B. M., Hitchens T. K., Meng W. S., Wesa A. K., Janjic J. M. A novel probe for the non-invasive detection of tumor-associated inflammation. Oncoimmunology. 2013; 2(2) e23034.

24. Ebner B., Behm P., Jacoby C., Burghoff S., French B. A., Schrader J., Flögel U. Early assessment of pulmonary inflammation by ^{19}F MRI in vivo. Circ. Cardiovasc. Imaging 2010; 3(2) 202-210.

25. Flögel U., Su S., Kreideweiß I., Ding Z., Galbarz L., Fu J., Jacoby C., Witzke O., Schrader J. Noninvasive detection of graft rejection by in vivo 19F MRI in the early stage. Am. J. Transplant. 2011; 11(2) 235-244.

26. Flögel U., Burghoff S., van Lent P. L., Temme S., Galbarz L., Ding Z., El-Tayeb A., Huels S., Bönner F., Borg N., Jacoby C., Müller C. E., van den Berg W. B., Schrader J. Selective activation of adenosine A2A receptors on immune cells by a CD73-dependent prodrug suppresses joint inflammation in experimental rheumatoid arthritis. Sci. Transl. Med. 2012; 4(146) 146ra108.

27. Hertlein T., Sturm V., Kircher S., Basse-Lusebrink T., Haddad D., Ohlsen K., Jakob P. Visualization of abscess formation in a murine thigh infection model of Staphylococcus aureus by ^{19}F-magnetic resonance imaging (MRI). PLoS One 2011; 6(3) e18246.

28. Hitchens T. K., Ye Q., Eytan D. F., Janjic J. M., Ahrens E. T., Ho C. ^{19}F MRI detection of acute allograft rejection with in vivo perfluorocarbon labeling of immune cells. Magn Reson. Med. 2011; 65(4) 1144-1153.

29. Hockett F. D., Wallace K. D., Schmieder A. H., Caruthers S. D., Pham C. T., Wickline S. A., Lanza G. M. Simultaneous dual frequency 1H and 19F open coil imaging of arthritic rabbit knee at 3T. IEEE Trans. Med. Imaging 2011; 30(1) 22-27.

30. Jacoby C., Borg N., Heusch P., Sauter M., Bönner F., Kandolf R., Klingel K., Schrader J., Flögel U. Visualization of immune cell infiltration in experimental viral myocarditis by ^{19}F MRI in vivo. Magn. Reson. Mater. Phy. 2013; 27(1):101-6.

31. Kadayakkara D. K., Ranganathan S., Young W. B., Ahrens E. T. Assaying macrophage activity in a murine model of inflammatory bowel disease using fluorine-19 MRI. Lab Invest 2012; 92(4) 636-645.

32. van Heeswijk R. B., De B. J., Kania G., Gonzales C., Blyszczuk P., Stuber M., Eriksson U., Schwitter J. Selective in vivo visualization of immune-cell infiltration in a mouse model of autoimmune myocarditis by fluorine-19 cardiac magnetic resonance. Circ. Cardiovasc. Imaging 2013; 6(2) 277-284.

33. Weise G., Basse-Luesebrink T. C., Wessig C., Jakob P. M., Stoll G. In vivo imaging of inflammation in the peripheral nervous system by (19)F MRI. Exp. Neurol. 2011; 229(2) 494-501.

34. Partlow K. C., Chen J., Brant J. A., Neubauer A. M., Meyerrose T. E., Creer M. H., Nolta J. A., Caruthers S. D., Lanza G. M., Wickline S. A. ^{19}F magnetic resonance imaging for stem/progenitor cell tracking with multiple unique perfluorocarbon nanobeacons. FASEB J. 2007; 21(8) 1647-1654.

35. Ostrowsky N. Liposome size measurements by photon correlation spectroscopy. Chem. Phys. Lipids 1993; 64(1-3) 45-56.

36. O'Hagan D. Understanding organofluorine chemistry. An introduction to the C-F bond. Chem. Soc. Rev. 2008; 37(2) 308-319.

37. Riess J. G. Oxygen carriers ("blood substitutes")--raison d'etre, chemistry, and some physiology. Chem. Rev. 2001; 101(9) 2797-2920.

38. Clark L. C., Jr., Gollan F. Survival of mammals breathing organic liquids equilibrated with oxygen at atmospheric pressure. Science 1966; 152(3730) 1755-1756.

39. Vorobév S. I. First- and second-generation perfluorocarbon emulsions. Pharm. Chem. J. 2009; 43(4) 30-40.

40. Jacoby C., Temme S., Mayenfels F., Benoit N., Krafft M. P., Schubert R., Schrader J., Flögel U. Probing different perfluorocarbons for in vivo inflammation imaging by ^{19}F MRI: Image reconstruction, biological half-lives, and sensitivity. NMR Biomed. 2013; 27(3):261-71

41. Bertilla S. M., Thomas J. L., Marie P., Krafft M. P. Cosurfactant effect of a semifluorinated alkane at a fluorocarbon/water interface: impact on the stabilization of fluorocarbon-in-water emulsions. Langmuir 2004; 20(10) 3920-3924.

42. Benita S. Submicron Emulsions in Drug Targeting and Delivery. Boca Raton (Florida, USA): CRC Press; 1998.

43. Nel A. E., Madler L., Velegol D., Xia T., Hoek E. M., Somasundaran P., Klaessig F., Castranova V., Thompson M. Understanding biophysicochemical interactions at the nano-bio interface. Nat. Mater. 2009; 8(7) 543-557.

44. Champion J. A., Mitragotri S. Role of target geometry in phagocytosis. Proc. Natl. Acad. Sci. U. S. A 2006; 103(13) 4930-4934.

45. Dos S. T., Varela J., Lynch I., Salvati A., Dawson K. A. Quantitative assessment of the comparative nanoparticle-uptake efficiency of a range of cell lines. Small 2011; 7(23) 3341-3349.

46. Allen T. M., Brandeis E., Hansen C. B., Kao G. Y., Zalipsky S. A new strategy for attachment of antibodies to sterically stabilized liposomes resulting in efficient targeting to cancer cells. Biochim. Biophys. Acta 1995; 1237(2) 99-108.

47. Owens D. E. III, Peppas N. A. Opsonization, biodistribution, and pharmacokinetics of polymeric nanoparticles. Int. J. Pharm. 2006; 307(1) 93-102.

48. Wen A. M., Lee K. L., Yildiz I., Bruckman M. A., Shukla S., Steinmetz N. F. Viral nanoparticles for in vivo tumor imaging. J. Vis. Exp. 2012; (69) e4352.

49. Diou O., Tsapis N., Giraudeau C., Valette J., Gueutin C., Bourasset F., Zanna S., Vauthier C., Fattal E. Long-circulating perfluorooctyl bromide nanocapsules for tumor imaging by 19F MRI. Biomaterials 2012; 33(22) 5593-5602.

50. Steenpaß T. PEGylated steroles for functionalization of liposomal surfaces. Thesis, Albert Ludwigs University; Freiburg 2004.

51. Giraudeau C., Djemai B., Ghaly M. A., Boumezbeur F., Meriaux S., Robert P., Port M., Robic C., Le B. D., Lethimonnier F., Valette J. High sensitivity ^{19}F MRI of a perfluorooctyl bromide emulsion: application to a dynamic biodistribution study and oxygen tension mapping in the mouse liver and spleen. NMR Biomed. 2012; 25(4) 654-660.

52. Kaneda M. M., Caruthers S., Lanza G. M., Wickline S. A. Perfluorocarbon nanoemulsions for quantitative molecular imaging and targeted therapeutics. Ann. Biomed. Eng 2009; 37(10) 1922-1933.

53. Giraudeau C., Geffroy F., Meriaux S., Boumezbeur F., Robert P., Port M., Robic C., Le B. D., Lethimonnier F., Valette J. ^{19}F molecular MR imaging for detection of brain tumor angiogenesis: in vivo validation using targeted PFOB nanoparticles. Angiogenesis. 2013; 16(1) 171-179.

54. Bae P. K., Jung J., Lim S. J., Kim D., Kim S. K., Chung B. H. Bimodal perfluorocarbon nanoemulsions for nasopharyngeal carcinoma targeting. Mol. Imaging Biol. 2013; 15(4) 401-410.

55. Wang X., Hagemeyer C. E., Hohmann J. D., Leitner E., Armstrong P. C., Jia F., Olschewski M., Needles A., Peter K., Ahrens I. Novel single-chain antibody-targeted microbubbles for molecular ultrasound imaging of thrombosis: validation of a unique noninvasive method for rapid and sensitive detection of thrombi and monitoring of success or failure of thrombolysis in mice. Circulation 2012; 125(25) 3117-3126.

56. Srinivas M., Morel P. A., Ernst L. A., Laidlaw D. H., Ahrens E. T. Fluorine-19 MRI for visualization and quantification of cell migration in a diabetes model. Magn Reson. Med. 2007; 58(4) 725-734.

57. Srinivas M., Turner M. S., Janjic J. M., Morel P. A., Laidlaw D. H., Ahrens E. T. In vivo cytometry of antigen-specific t cells using ^{19}F MRI. Magn Reson. Med. 2009; 62(3) 747-753.

58. Waiczies H., Lepore S., Janitzek N., Hagen U., Seifert F., Ittermann B., Purfurst B., Pezzutto A., Paul F., Niendorf T., Waiczies S. Perfluorocarbon particle size influences magnetic resonance signal and immunological properties of dendritic cells. PLoS One 2011; 6(7) e21981.